12th International Conference on Fracture Mechanics of Concrete and Concrete Structures
FraMCoS-12
B.L.A. Pichler, Ch. Hellmich, P. Preinstorfer (Eds)

https://doi.org/10.21012/FC12.1124
MS05-2:4

NUMERICAL SIMULATION OF BUBBLEDEC TYPE REINFORCED CONCRETE SLABS SUBJECTED TO PUNCHING LOADING CONDITIONS

JOAQUIM A. O. BARROS[*†], **WANDERLEY G. NICÁCIO** [††], **A. VENTURA-GOUVEIA**[*†††], **FÁBIO P. FIGUEIREDO**[*††††]

[*]ISISE, Dep. Civil Engineering, University of Minho, Portugal, e-mail: [†]barros@civil.uminho.pt

[††]Federal Institute of Education, Science and Technology, Brazil, e-mail: wanderley.nicacio@gmail.com

[†††]Dep. Civil Engineering, Polytechnic Institute of Viseu, Portugal, e-mail: ventura@estgv.ipv.pt

[††††]AtkinsRéalis, UK, e-mail: Fabio.Figueiredo@atkinsrealis.com

Key words: BubbleDeck slab, Punching, Nonlinear finite element analysis, Multidirectional fixed smeared crack model

Abstract: BubbleDeck type slab (BD) is a lightweight construction system for building floors where recycled plastic hollow spheres (RPHS) are disposed in its core to decrease its deadweight without significant loss of stiffness, flexural and shear strength. However, the behaviour of BD under punching loading conditions is not yet well known, despite its use in real practice has increased significantly in the last years. Since punching is a brittle failure mode, in this work an experimental program with BD prototypes is complemented with advanced numerical simulations to assess not only the punching capacity of BD but also to explore the potential of nonlinear finite element analysis on the simulation of this complex structural system. When compared to the equivalent solid RC slabs (SS), the experimental tests showed a smaller performance in terms of punching capacity and ductility. Regarding the numerical simulations, a multidirectional fixed smeared crack model applied to a refined finite element mesh where concrete was simulated by solid finite elements, and steel reinforcements were considered perfectly bonded, was demonstrated capable of capturing the main experimental records, namely the load vs deflection and strains in the constituent materials. This demonstrates that this numerical approach can be explored to optimize numerically the BD to have larger punching capacity and ductility, such is the case of using fibre reinforced concrete.

1 INTRODUCTION

BubbleDeck slab (BD) is a slab system where recycled plastic hollow spheres (RPHS) are used to decrease its deadweight over conventional solid reinforced concrete (RC) slabs (SS) without significant loss of flexural stiffness [1,2]. The RPHS are disposed in the core of the BD slab and maintained in their position using top and bottom steel grid mesh, giving the slab an orthotropic behaviour in terms of stiffness. Prefabricated RC panels have also been used in the bottom part of BD, as non-recoverable moulds, for speeding up the construction process of this slab system [3]. The presence of RPHS, however, introduces some concerns in terms of the punching resistance of BD. In fact, experimental evidence has demonstrated that BD fails in punching with a smaller load carrying capacity than their SS counterparts, even when RPHS are not used in the vicinity of the supporting column [4]. Using steel girders in the solid zones of a BD system has increased the punching capacity by 30% [5].

An experimental program with BD and SS slab prototypes, including, or not, prefabricated RC panels (when including it was adopted the designation BDP and SSP), was executed under loading and support conditions to promote punching failure mode [6]. It was verified that all tested slab prototypes failed in punching with a decrease of the punching capacity in the BD over the corresponding SS between 4 and 14%, and a reduction in the deflection at failure between 8% and 44%. By considering the ductility index (μ) as the ratio between the deflection at peak load versus the deflection at yield initiation of the tensile flexural reinforcement, BD slab prototypes presented μ values smaller than the recommended minimum [7].

In this work, the potential of the reinforcement of steel fibres to increase the punching capacity and ductility of BD slabs is explored by performing nonlinear finite element analysis. For this purpose, initially, the predictive performance of a 3D multidirectional fixed smeared crack model (MDFSCM) [8] is assessed by simulating the slab prototypes tested elsewhere [6]. After demonstrating the suitability of the adopted MDFSCM in predicting the relevant behavioural aspects of the experimentally tested BD and SS, the use of steel fibre reinforced concrete (SFRC) for eliminating the conventional punching reinforcement and ensuring flexural failure mode is investigated numerically.

2 Experimental program

2.1 Introduction

In this section a concise description of the experimental program is provided to properly contextualize the numerical simulations in the next section. Further information can be found elsewhere [6].

2.2 Slab specimens

The experimental program is composed of four flat reinforced concrete (RC) slab prototypes (Fig. 1): a) a solid slab (SS); b) a solid slab with a bottom RC precast layer (SSP); c) *BubbleDeck* slab (BD); d) BD slab with a bottom RC precast layer (BDP). Their geometry is shown in Fig. 2 and the configurations of the reinforcements are provided in Fig. 3.

2.3 Properties of the materials

The properties of the concrete (average compressive strength, f_{cm}, average splitting tensile strength, $f_{t,Dm}$, and average Young's modulus, E_{cm}, and their coefficient of variation, CoV), determined at the age of testing the slab prototypes, are indicated in Table 1. The tensile properties of the steel bars constituting the reinforcements (average modulus of elasticity, E_{sm}, average stress at yield initiation, f_{ysm}, average strain and yield initiation, ε_{ysm}, and their CoV) are provided in Table 2.

Table 1: Concrete properties.

Slab	f_{cm} (MPa)	CoV (%)	$f_{t,Dm}$ (MPa)	CoV (%)	E_{cm} (GPa)	CoV (%)
Precast layer	34.9	5.7	3.6	5.3	28.3	8.5
SS and SSP	44.6	5.7	3.8	3.0	28.6	8.6
BD and BDP	47.0	9.1	3.0	8.1	28.6	13.9

Table 2: Properties of steel reinforcements.

Property	Type of reinforcement				
	Mesh		Bar		
	Diameter (mm)		Diameter (mm)		
	6	8	8	10	12.5
E_{sm} (GPa)	190 (4.1%)	194 (3%)	196 (3.5%)	193 (3.9%)	183 (2.8%)
f_{ysm} (MPa)	627 (0.7%)	681 (1.6%)	675 (6.8%)	618 (1.1%)	577 (0.2%)
ε_{ysm} (‰)	3.3 (4.6%)	3.5 (1.8%)	3.4 (3.3%)	3.2 (3.2%)	3.1 (3.0%)

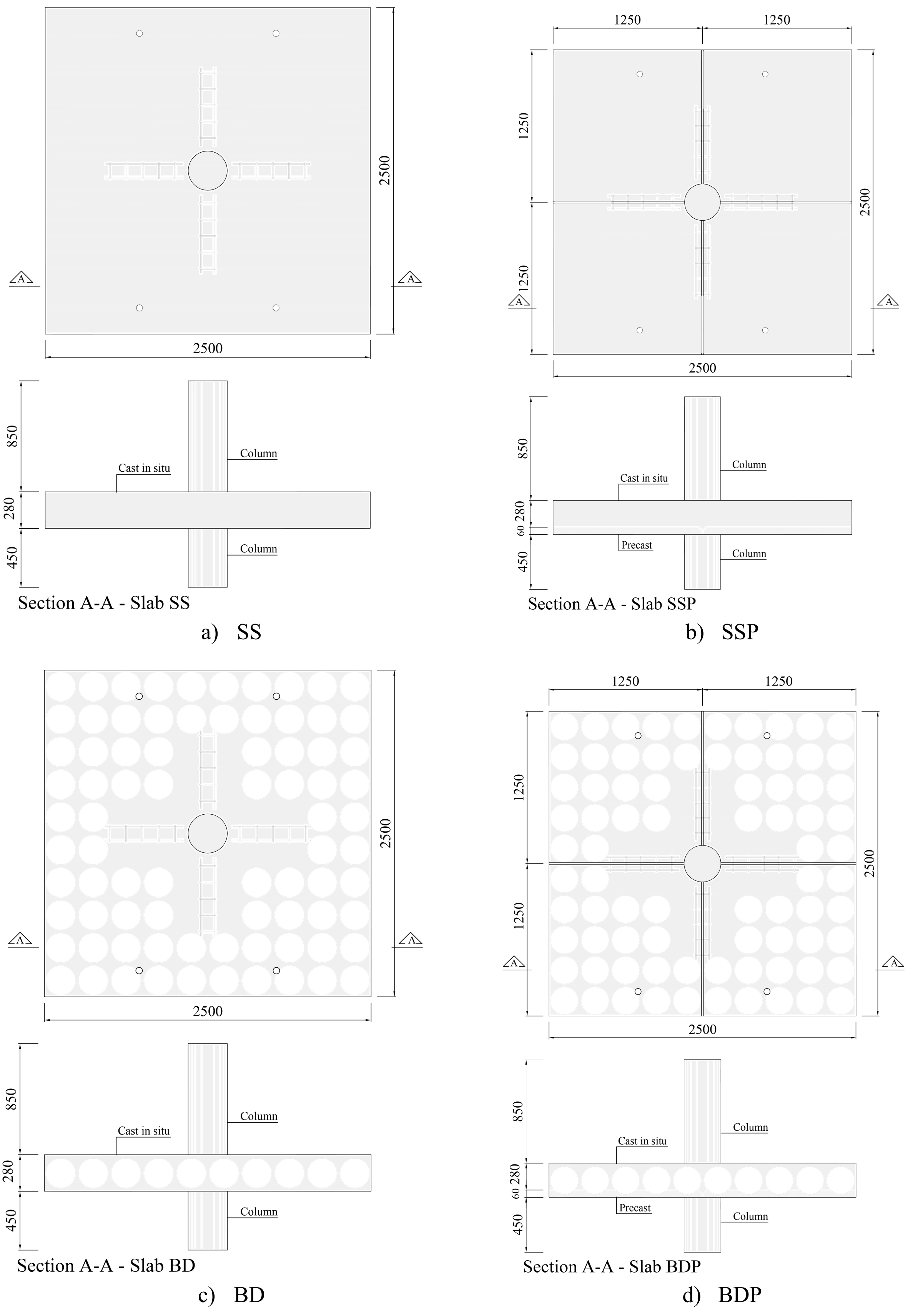

Fig. 1: Slab prototypes of the experimental program (dimensions in mm).

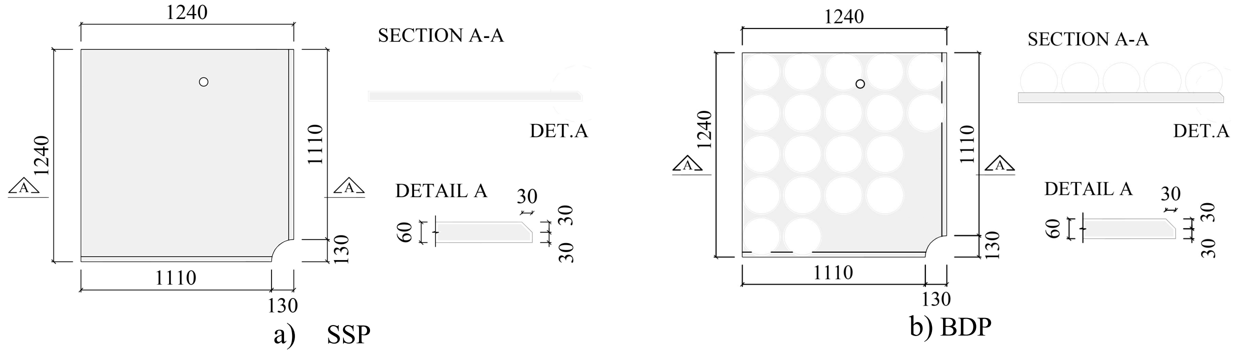

Fig. 2: Geometry of the RC precast layer (dimensions in mm).

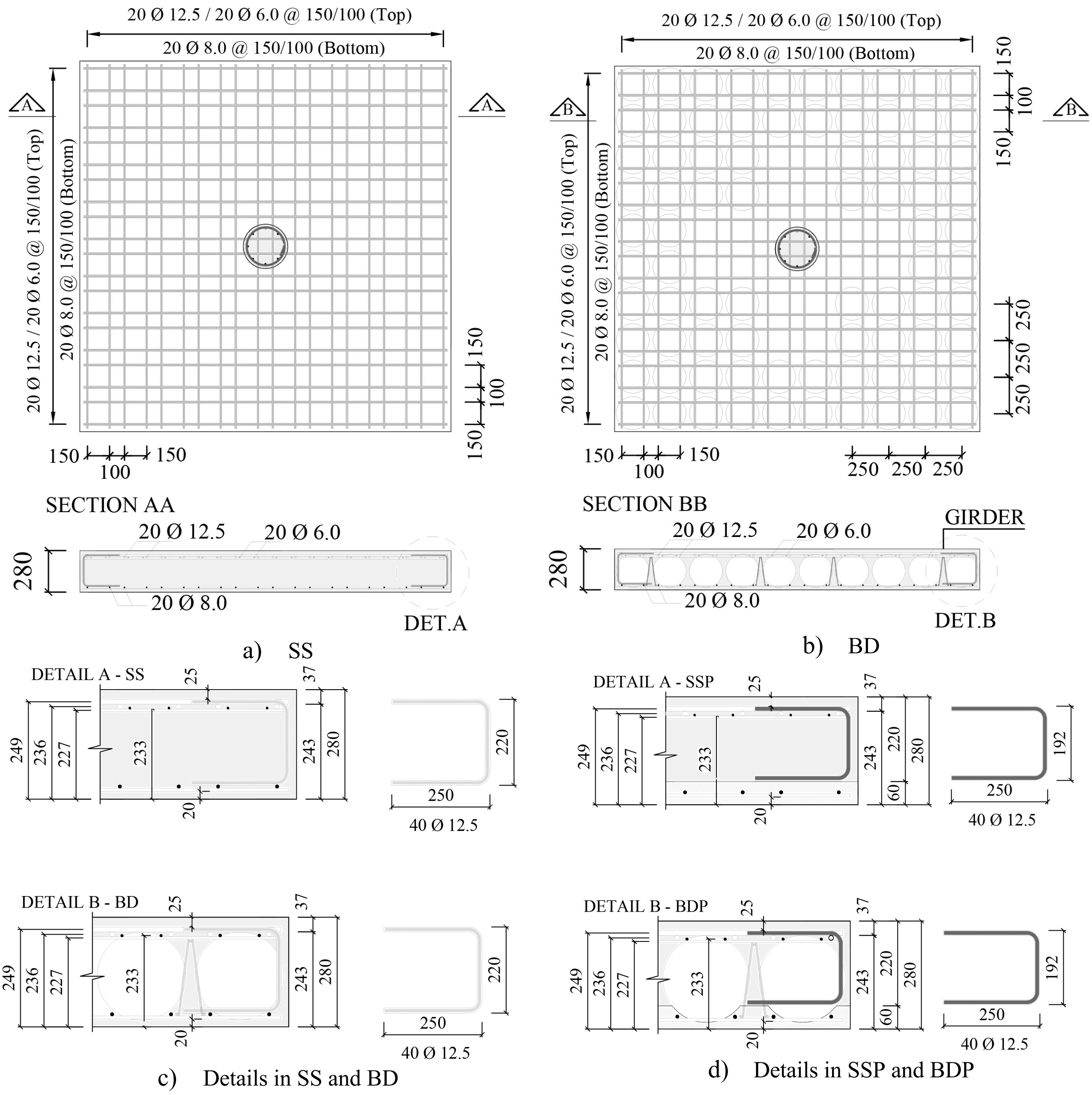

Fig. 3: Reinforcements (dimensions in mm).

2.4 Test setup and monitoring systems

Fig. 4 shows the test setup adopted in the experimental program. The loading system is composed of four hydraulic actuators, each one equipped with a load cell. These actuators apply the load to a steel profile, which transfers this load to the slab in two zones of 140×140mm^2 contact area. A prototype is subjected to 8 of these load contact areas. Figure 5 presents the localization of the displacement transducers (LVDT) to monitor the slab's deflection, the location of the strain gauges to record the strains in the top flexural reinforcement, SSF1 to SSF6, and in the punching shear reinforcement (middle depth of the legs), SSS1 to SSS6, and the radial and circumferential strains in the concrete bottom's slab surface, CRS and CCS, respectively.

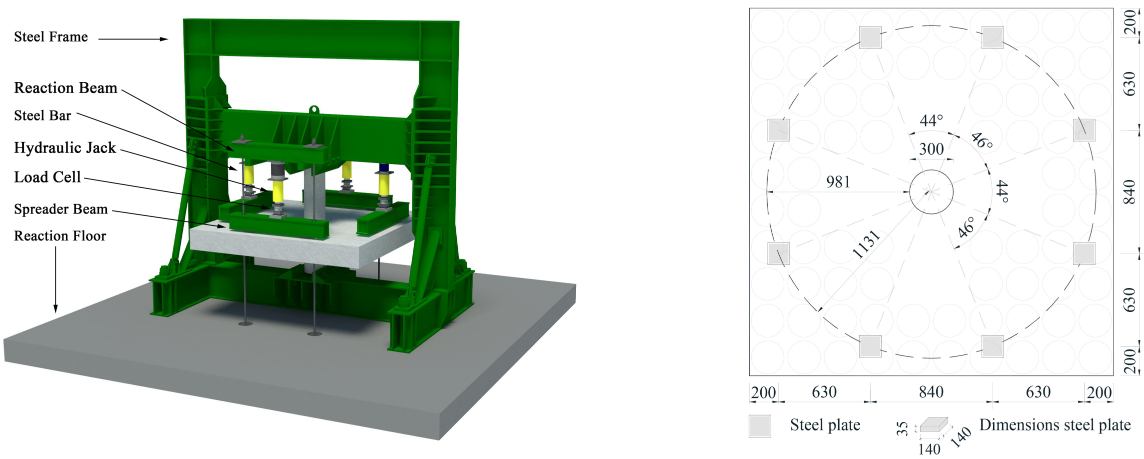

a) Reaction frame b) Loaded zones (dimensions in mm)

Fig. 4: Test setup.

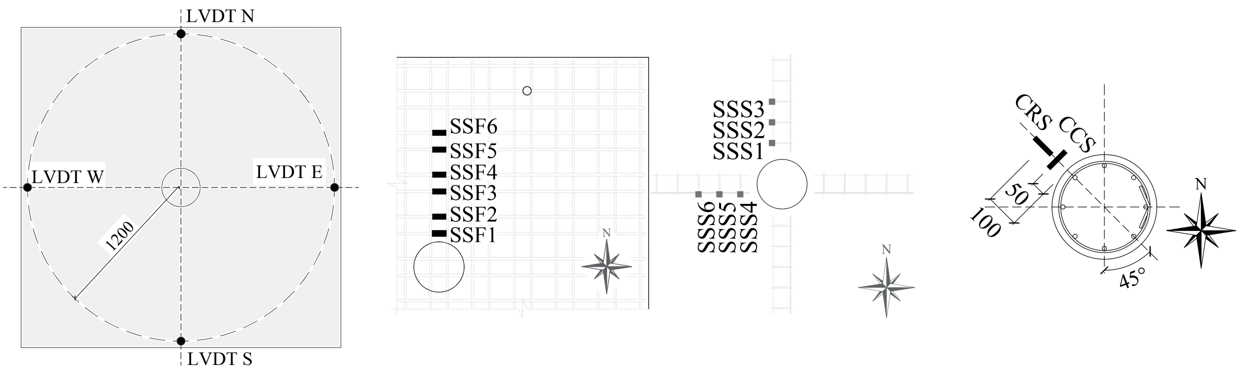

a) Slab's deflection b) Strains in the reinforcements c) Strain in the concrete

Fig. 5: Monitoring system.

2.5 Relevant results

The punching capacity and the deflection at failure of BD have decreased up to 14% and 44%, respectively, when compared to the corresponding SS (Table 3). $V_{\max}^{SSP(BDP)}$ and $V_{\max}^{SS(BD)}$ are the load carrying capacity of the SS and BD with, and without, respectively, the precast RC plates. A relatively small ductility index was obtained (between 1.51 and 2.65).

Table 3: Relevant results.

Slab	$V_{\max}$	$\frac{V_{\max}^{SSP(BDP)}-V_{\max}^{SS(BD)}}{V_{\max}^{SS(BD)}}$	$\frac{V_{\max}^{BDi}-V_{\max}^{SSi}}{V_{\max}^{SSi}}$	$\delta_{V_{\max}}$	$\frac{\delta_{V_{\max}}^{SSP(BDP)}-\delta_{V_{\max}}^{SS(BD)}}{\delta_{V_{\max}}^{SS(BD)}}$	$\frac{\delta_{V_{\max}}^{BDi}-\delta_{V_{\max}}^{SSi}}{\delta_{V_{\max}}^{SSi}}$
	(kN)	(%)	(%)	(mm)	(%)	(%)
SS	1041	-	-	17.1	-	-
SSP	987	-5.2	-	22.4	31.0	-
BD	995	-	-4.4	15.8	-	-7.6
BDP	846	-15.0	-14.3	12.6	-20.3	-43.8

All the tested slabs failed in punching after the occurrence of yield initiation of the flexural reinforcement.

3 NUMERICAL SIMULATIONS

3.1 Introduction

A 3D multidirectional fixed smeared crack model (MDFSCM) is assessed by modelling the relevant behavioural aspects of the slab prototypes of the experimental program described in the previous section.

3.2 Model description

The MDFSCM is implemented in the FEMIX computer program [9] whose complete description can be found elsewhere [8]. Herein a short description of this model is provided for a comprehensive understanding of the analyses carried out and the values adopted for the model parameters. This description will be made at the level of an integration point (IP). According to the MDFSCM:

$$\Delta\underline{\varepsilon} = \Delta\underline{\varepsilon}^{co} + \Delta\underline{\varepsilon}^{cr} \quad (1)$$

where $\Delta\underline{\varepsilon}$, $\Delta\underline{\varepsilon}^{co}$ and $\Delta\underline{\varepsilon}^{cr}$ are the incremental strain vector in the cracked concrete, in the intact concrete and in the smeared cracks, respectively. The constitutive law for the cracked concrete is:

$$\Delta\underline{\sigma} = \left(\underline{D}^{co} - \underline{D}^{co}\left[\underline{T}^{cr}\right]^T \left(\underline{D}^{cr} + \underline{T}^{cr}\underline{D}^{co}\left[\underline{T}^{cr}\right]^T \right)^{-1} \underline{T}^{cr}\underline{D}^{co} \right)\Delta\underline{\varepsilon} \quad (2)$$

where $\underline{D}^{co}$ is the constitutive matrix according to Hooke's law, dependent on the concrete Young's modulus (E_c) and Poisson's ratio (ν_c), $\underline{T}^{cr}$ is the transformation matrix between entities in the coordinate systems of the cracks formed in the IP (several cracks can be formed in the MDFSCM, according to the criterion adopted for crack formation) and the global coordinate system (Fig. 6), and $\underline{D}^{cr}$ represents the crack constitutive matrix:

$$\underline{D}^{cr} = \begin{bmatrix} D_n^{cr} & 0 & 0 \\ 0 & D_{t_1}^{cr} & 0 \\ 0 & 0 & D_{t_2}^{cr} \end{bmatrix} \quad (3)$$

where D_n^{cr}, $D_{t_1}^{cr}$ and $D_{t_2}^{cr}$ represent, respectively, the fracture mode I (in $\hat{n}$ direction, normal to the crack plane), mode II (in $\hat{t}_1$ sliding direction) and mode III (in the $\hat{t}_2$ sliding direction) moduli.

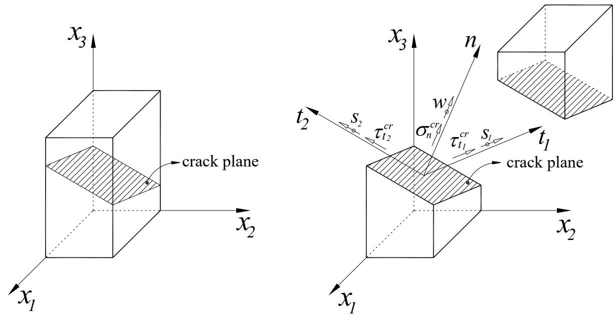

Fig. 6 - Crack stress components, displacements and crack local coordinate system (only one crack is assumed formed in the IP).

The concrete between cracks is assumed to have linear-elastic behaviour, as supported by experimental evidence in slabs failing in punching [10]. The multilinear diagram represented in Fig. 7a was used to simulate D_n^{cr}, where f_{ct} is the concrete tensile strength, G_{fI} is the concrete mode I fracture energy, and l_b represents the length of the portion of material representative of the IP where G_{fI} is dissipated, in an attempt to provide results that are independent of the finite element (FE) mesh refinement. In the present numerical simulations l_b was considered equal to $\sqrt[3]{V_{IP}}$, where V_{IP} is the volume of the IP. Previous research has demonstrated the mesh objectivity of the adopted model [11]. For modelling the crack shear sliding components ($D_{t_1}^{cr}$ and $D_{t_2}^{cr}$), the crack shear softening diagram shown in Fig. 7b was adopted, where the initial shear fracture modulus, $D_{t,1}^{cr} = \beta/(1-\beta)G_c$, depends on the value attributed to the shear retention factor, $\beta \in]0,1[$, and the concrete elastic shear modulus, $G_c = E_c/\left(2(1+\upsilon_c)\right)$. The other parameters are the crack shear strength, $\tau_{t,p}^{cr}$, the fracture energy in modes II and III, $G_{f,s}$, (considered equal for both fracture modes), and the crack bandwidth (assumed equal to the approach adopted to define the l_b for the mode I fracture energy).

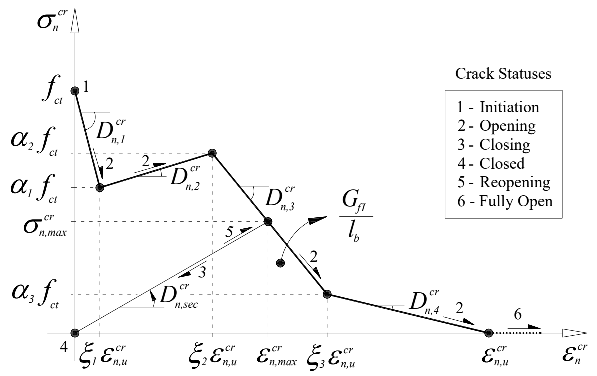

a) Fracture mode I

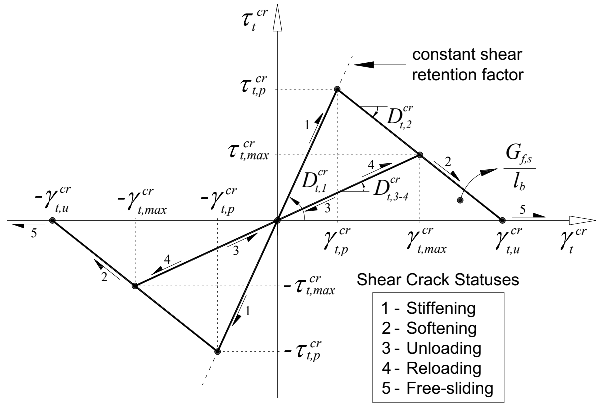

b) Fracture modes II and III

Fig. 7 - Diagrams to simulate the cracking process.

The reinforcements were simulated as embedded cables, with perfect bond to the surrounding concrete, using the stress-strain diagram represented in Fig. 8.

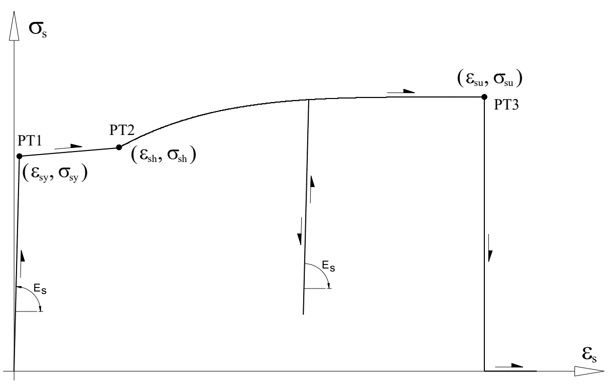

Fig. 8 - Stress-strain diagram for modelling the reinforcements.

Springs were adopted to simulate the part of the column that transferred the load from the slab to the support reaction system, by using a force *vs* displacement response governed by the diagram shown in Fig. 9.

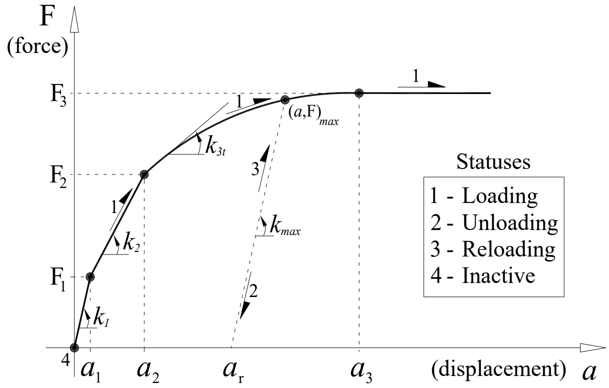

Fig. 9 - Force-displacement diagram adopted for modelling the springs simulating the slab's column and its contact with the support reaction system.

3.3 Finite element mesh and values of the model's parameters

Taking advantage of the double symmetry structural conditions of the tested slabs, only one-quarter of the slab was simulated. The FE mesh, loading and support conditions for the SS and BD type slabs are shown in Figs. 10 and 11, respectively. Due to identical reasons, the top part of the column was also not included in the FE meshes.

For modelling the SS type slabs, solid Serendipity 20 node FE, with Gauss-Legendre (GL) integration scheme of 2×2×2 were adopted, while for the BD type slabs, due to the much higher number of FE required for attending their geometric complexities, solid Lagrangian 8 node FE, with the same integration scheme, were considered. In both types of slabs, the reinforcements were simulated by 3D linear embedded cables of 2 nodes and with GL integration scheme of 2 IPs. The values of the model parameters adopted in the numerical simulations are included in Tables 4, 5 and 6 for the concrete, reinforcements and springs, respectively. These values are obtained from the results registered in the experimental tests with the concrete and reinforcements, and considering the recommendations of the CEB-FIP model code 2010 (MC2010) for the fracture mode I parameters. For the values that define the fracture mode II and III parameters (Fig. 7b) the recommendations elsewhere [12] were considered.

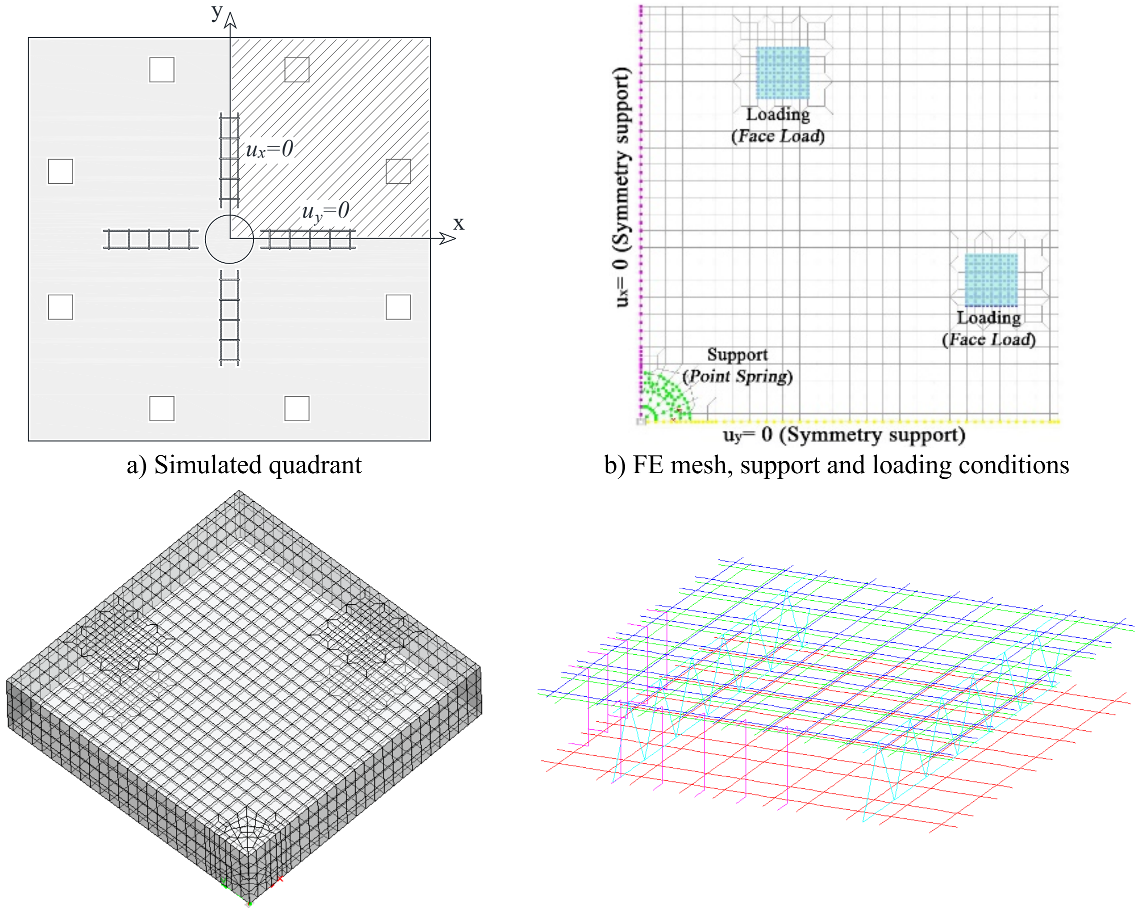

a) Simulated quadrant b) FE mesh, support and loading conditions

c) Isometric view of the FE mesh d) Steel reinforcements (red: ϕ8mm, green: ϕ6mm, blue: ϕ12.5mm, cyan: ϕ4.2mm, violet: ϕ8mm)

Fig. 10: Modelling attributes of the SS type slabs.

Table 4: Concrete constitutive model values (Fig. 7).

Property	Value
Poisson's ratio (ν_c)	0.10
Initial Young's modulus (E_c , GPa)	26 (BD and BDP), 28 (SS and SSP)
Tri-linear crack normal stress *vs* crack normal strain diagram and quadri-linear for the SFRC (Fig. 7a)	f_{ct} (MPa)= 2.2 (SS and BD), 2 (SSP), 1.8 (BDP cast in place concrete), 2.2 (BDP Precast layer), 2 (SSP cast in place concrete), 2 (SSP Precast layer), 2.2 (SFRC); G_{fI} (N/mm)=0.07, 4.32 (SFRC); ξ_1=0.005, 0.0025 (SFRC); α_1 = 0.4, 0.539 (SFRC); ξ_2=0.2, 0.285 (SFRC); α_2 = 0.15, 0.691 (SFRC); ξ_3=0.759 (SFRC); α_3 = 0.561 (SFRC)
Bilinear crack shear stress *vs* crack shear strain diagram (Fig. 7b)	β =0.1, 0.2 (SFRC); $\tau_{t,p}^{cr}$ (MPa)=1, 2 (SFRC); $G_{f,s}$ (N/mm)=0.25, 0.5 (SFRC)
Crack bandwidth	$l_b = \sqrt[3]{V_{IP}}$
Threshold angle	α_{th} = 30º
Maximum number of SC per IP	2

Table 5: Values for modelling the reinforcements (Fig. 8) (*p*=1 considers a linear PT2-TP3 branch).

Bar diameter (mm)	Property						
	ε_{sy} (‰)	σ_{sy} (MPa)	ε_{sh} (‰)	σ_{sh} (MPa)	ε_{su} (‰)	σ_{su} (MPa)	*p*
6.0	3.3	527	50	650	60	650	1
8.0	3.4	630	30	697	50	697	1
12.5	3.1	481	19	700	20	700	1

Table 6: Values for modelling the springs (Fig. 9).

Slabs	Property						
	n° springs	F_1 (N)	F_2 (N)	F_3 (N)	a_1 (mm)	a_2 (mm)	a_3 (mm)
SS and SSP	32	1197	4788	24298	0.500	1.250	2.326
BD and BDP	56	684	2736	13884	0.500	1.250	2.326

In the MDFSCM, average strains and average stresses are determined for the reinforcement. However, since in the cracked section, the strain and corresponding stress are higher than the average values, the stress-strain relationship for the flexural reinforcement was adapted according to the recommendations proposed elsewhere [13].

The values that define the first two branches of the force-displacement diagram that simulate the springs (Fig. 9, Table 6) were obtained by inverse analysis by fitting the initial deformational stage of the experimentally tested slabs. The last branch of this diagram simulates the axial stiffness of the column.

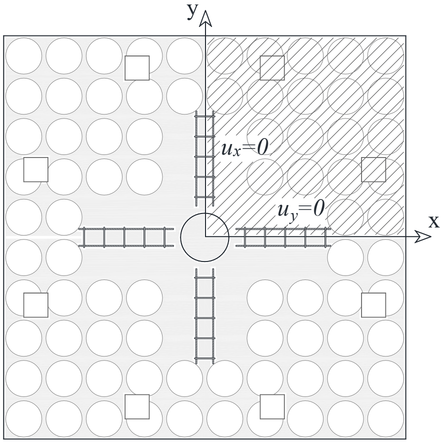

a) Simulated quadrant

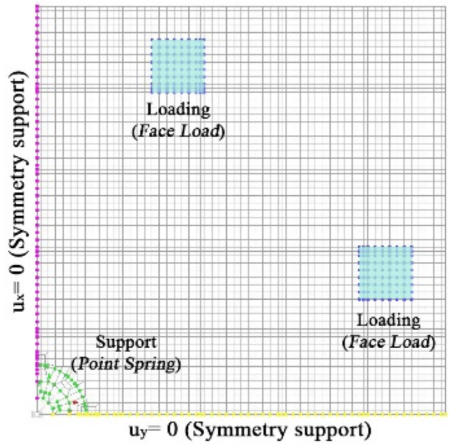

b) FE mesh, support and loading conditions

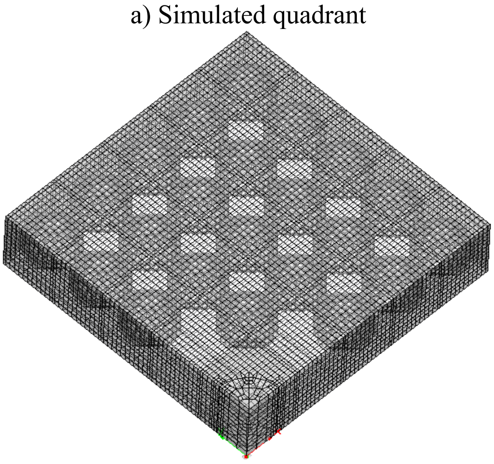

c) Isometric view of the FE mesh

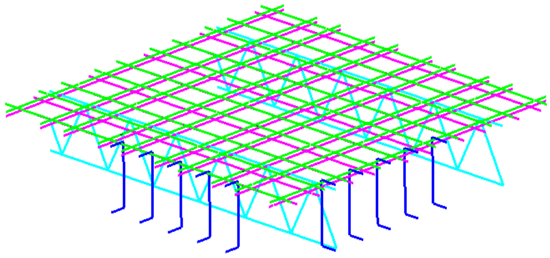

d) Steel reinforcements

Fig. 11: Modelling attributes of the BD type slabs.

3.4 Results and discussion

Fig. 12 compares the experimental and the numerical load versus average deflection in the slabs. The response was well captured up to the stage where convergence was no longer possible to ensure. The average error on the prediction of the maximum load carrying capacity of the slabs was about 4%, while apart from SSP, the average error on the deflection at maximum load was about 8%. In the experimental test of the SSP, at a load of 757 kN a significant loss of stiffness occurred, and the deflection at maximum load was significantly higher than the one registered in the other slabs (Table 3). The MDFSCM was not capable of capturing this relatively high deformability during the propagation of the punching failure. The experimental tests revealed that SSP developed a relatively larger perimeter failure surface with a dominance of flexural cracks [6]. The strains in the flexural reinforcements have also shown that at about 757 kN two bars have yielded followed by a progressive yielding of the remaining monitored bars. Therefore, this slab has experienced more inelastic deformation of the reinforcement than the other slabs, which may justify its higher deflection at failure. Fig. 13 compares relationships between the load and the strain in the SSF1 strain gauge registered experimentally and obtained numerically. The predictions were satisfactory, except the almost null variation of strain in BD and BDP when it was attained a strain of about 3‰. This was caused by a prediction of a crack pattern in the region where SSF1 was installed that was different from the one registered experimentally.

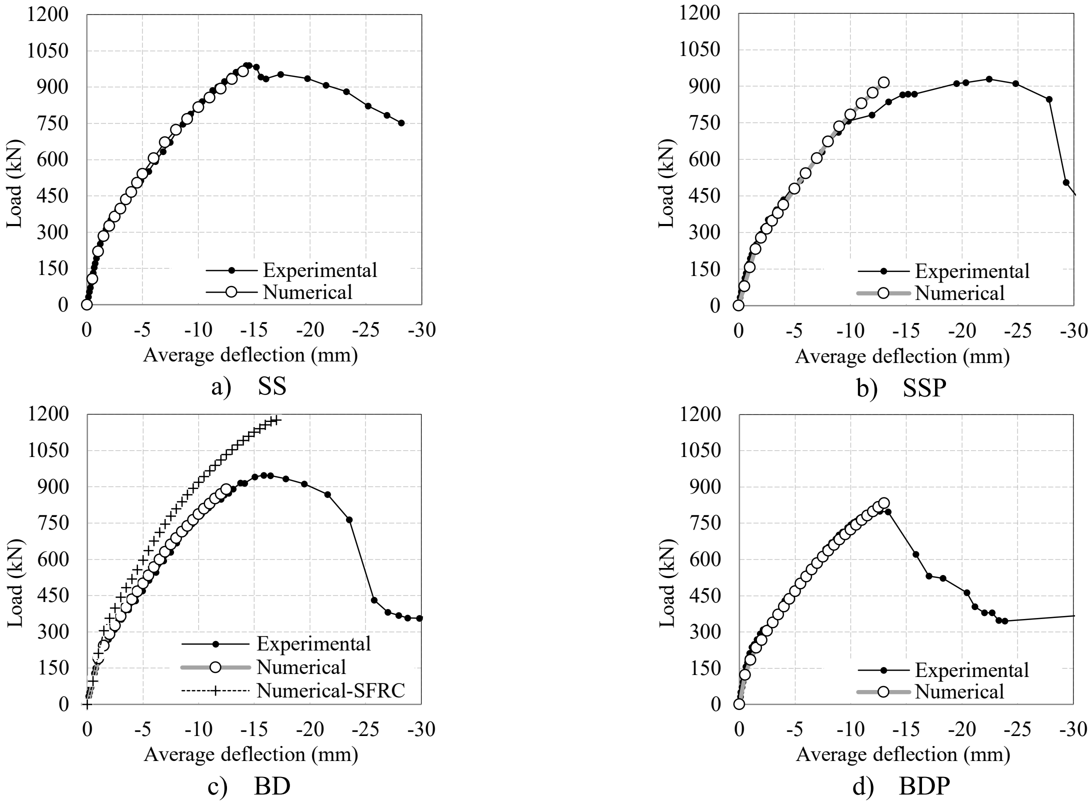

Fig. 12: Experimental and numerical load *vs* average deflection.

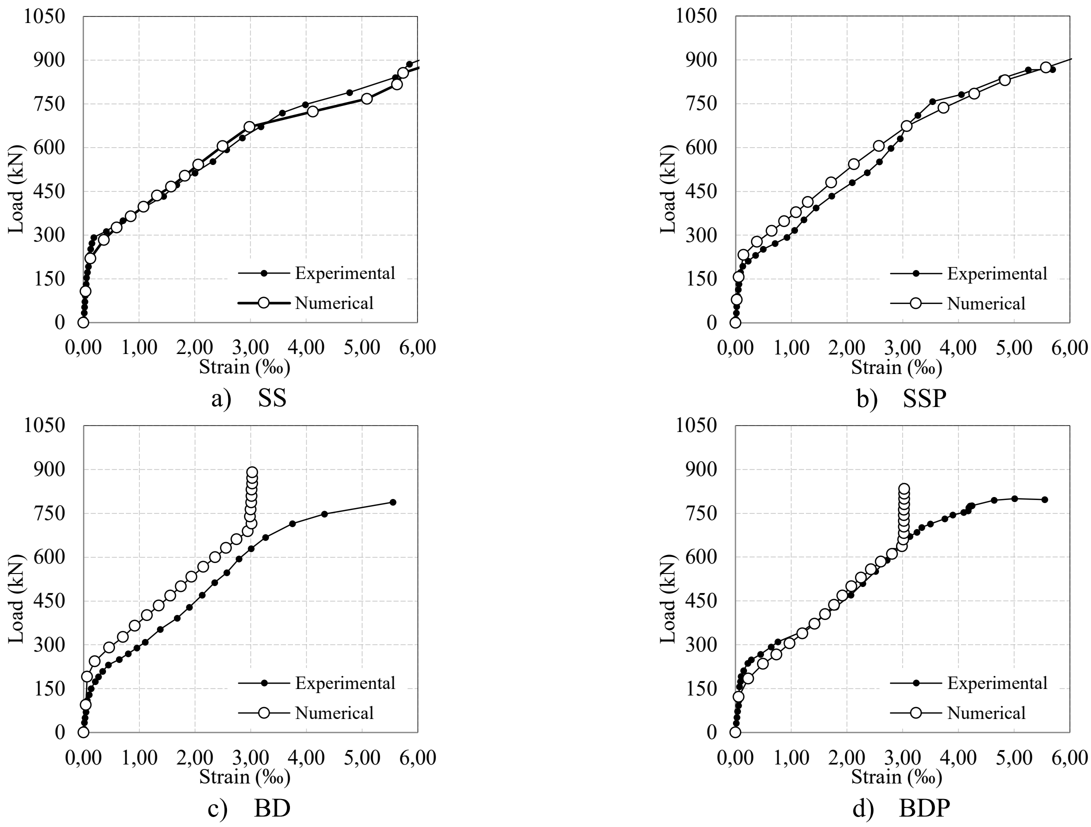

Fig. 13: Experimental and numerical load *vs* strain in the SSF1 of the flexural reinforcement (Fig. 5b).

The observed good predictive accuracy was also captured in terms of load versus radial and circumferential concrete strains (Fig. 14). However, the model was not capable of capturing the post-inflection stage registered experimentally in the radial strains, mainly in the BD series. Smaller circumferential strains were also predicted numerically in the SS slab, but the level of accuracy was quite acceptable considering the local character of the strains and the average strain concept adopted in the MDFSCM.

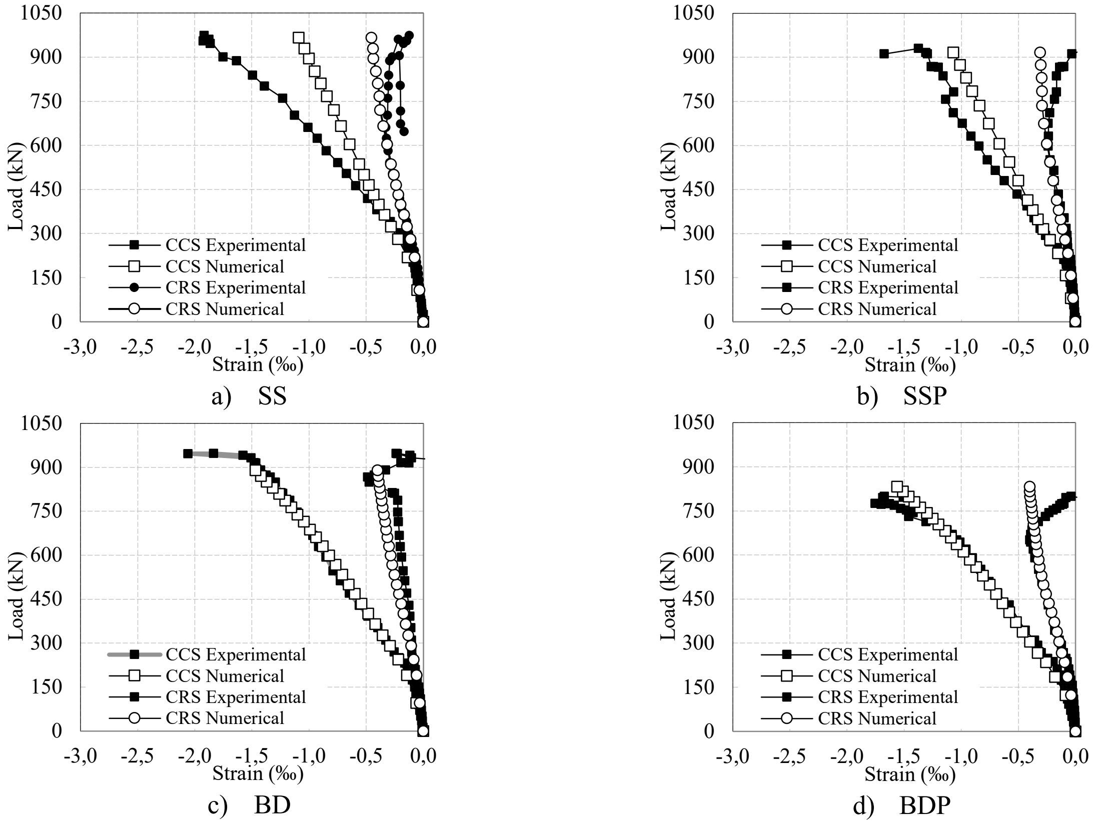

Fig. 14: Experimental and numerical load *vs* radial and circumferential strain in the concrete (Fig. 5c).

4 POTENTIAL OF SFRC AS A PUNCHING REINFORCEMENT

The possibility of eliminating the punching reinforcement with SFRC and assuring a flexural failure mode is assessed. For this purpose, an SFRC already adopted in another experimental program for assessing the potential of steel fibres as punching reinforcement [14], is considered in the simulations of the BD since it has the same strength class as the concrete adopted in BD prototypes. The properties are indicated in Table 4 (using SFRC designation). The force deflection obtained with this SFRC is included in Fig 12c, where it is verified that steel fibre reinforcement was able to increase the stiffness, load carrying capacity, and maximum deflection, but for the toughness class of the adopted SFRC was not yet possible to have a flexural failure more.

5 CONCLUSIONS

From the experimental results, it was verified that the tested slabs failed in punching. When compared to the SS type slabs, the BD have a decrease in the punching capacity from 4 to 14%, and from 8 to 44% in terms of deflection at failure. The precast RC panel decreased the punching capacity by 5% and 15% in SS and BD type slabs, respectively, while the decrease in terms of deflection was 31% and 20%. Regarding the numerical simulations, it was verified that the 3D multidirectional fixed smeared crack model could capture with good accuracy the force-deflection, and strains in the reinforcements and the concrete, but was not capable of reproducing the structural softening phase.

By using a steel fibre reinforced concrete (SFRC) already applied in RC slabs for increasing their punching capacity, it was verified numerically that this SFRC can replace the conventional punching reinforcement adopted in BD slab prototypes with benefits in terms, of stiffness, load carrying capacity and maximum deflection.

ACKNOWLEDGEMENTS

The authors acknowledge the support provided by FCT through the project TuRUpAI, DOI: 10.54499/2022.06602.PTDC, and PID2021-125553NB-I00 (MCI/AEI/FEDER, UE). This work was partly financed by FCT / MCTES through national funds (PIDDAC) under the R&D Unit Institute for Sustainability and Innovation in Structural Engineering (ISISE), under reference UIDB/04029/2020, and under the Associate Laboratory Advanced Production and Intelligent Systems ARISE under reference LA/P/0112/2020.

REFERENCES

[1] Bawens P.E., 1999. Bending strength and deflection behaviour - *Report from the Eindhoven Univ. Technology*, TU Eindhoven.

[2] Held M.S., 2002. Untersuchung an BubbleDeck Modulen - *Report from the Technical University of Darmstadt*, Darmstadt.

[3] Bubbledeck UK, 2008. BubbleDeck Voided Flat Slab Solutions - *Technical Manual & Documents*. BubbleDeck UK Head Office, Jersey. http://www.bubbledeck-uk.com/pdf/2-BDTechManualv1a.pdf [Accessed 15/12/2018].

[4] Held, M.S. and Pfeffer, K, 2002. Punching behavior of biaxial hollow slabs. *Cement and Concrete Composites*, **24**(6):551–556. doi.org/10.1016/S0958-9465(01)00071-3

[5] Ceballos, M.A., 2017. Experimental analysis of punching shear in BubbleDeck slabs with shear reinforcement. *Master's thesis*, University of Brasilia. Retrieved from http://repositorio.unb.br/handle/10482/24276.

[6] Nicácio, W.G., Barros, J.A.O., and Melo, G.S.S.A., 2020. Punching behavior of BubbleDeck type reinforced concrete slabs. *Structural Concrete - fib journal*, **21**(1), 262-277. doi.org/10.1002/suco.201900176

[7] Hashemi, S.S., Sadeghi, K., Vaghefi, M., and Siadat, S.A., 2018. Evaluation of Ductility of RC Structures Constructed with Bubble Deck System. International *Journal of Civil Engineering*, **16**(5), 513–526. doi.org/10.1007/s40999-017-0158-y.

[8] Ventura-Gouveia, A., Barros, J.A.O., and Azevedo, A.F.M., 2011. Crack constitutive model for the prediction of punching failure modes of fiber reinforced concrete laminar structures. *Computers & Concrete*, **8**(6), 735-755. doi.org/10.12989/cac.2011.8.6.735.

[9] Barros, J.A.O, 2016. Debilities and strengths of FEM-based constitutive models for the material nonlinear analysis of steel fiber reinforced concrete structures. In V. Saouma, J. Bolander and E. Landis (eds), California: *9th Inter. Conf. on Fract. Mech. of Conc. & Conc. Struct*. doi.org/10.21012/FC9.023.

[10] Muttoni A., 2008. Punching Shear Strength of Reinforced Concrete Slabs without Transverse Reinforcement. *ACI Structural Journal*; **105**:440–50. doi.org/10.14359/19858.

[11] Barros, J.A.O., Baghi, H., and Ventura-Gouveia, A., 2021. Assessing the applicability of a smeared crack approach for simulating the behaviour of concrete beams flexurally reinforced with GFRP bars and failing in shear. *Engineering Structures Journal*, **227**, 111391. doi.org/10.1016/j.engstruct.2020.111391

[12] Breveglieri, M., Barros, J.A.O., Aprile, A., and Ventura-Gouveia, A., 2016. Strategies for numerical modeling the behavior of RC beams strengthened in shear using the ETS technique. *Engineering Structures Journal*, **128**, 296-315. doi.org/10.1016/j.engstruct.2016.09.027.

[13] Stevens N.J., 1987. Analytical modeling of reinforced concrete subjected to monotonic and reversed loadings. *Publ No 87-1*.

[14] Barros, J.A.O. et al., 2024. Blind competition on the numerical simulation of slabs reinforced with conventional flexural reinforcement and fibres subjected to punching loading configuration. *fib Structural Concrete J*. doi.org/10.1002/suco.202400061